

# V2051 Oph’s disc evolution on decline from superoutburst

Sonja Vrielmann<sup>1,2\*</sup>, Warren Offutt<sup>3</sup>

<sup>1</sup>*Department of Astronomy, University of Cape Town, Private Bag, Rondebosch, 7700, South Africa (sonja@mensa.ast.uct.ac.za)*

<sup>2</sup>*Hamburger Sternwarte, Universität Hamburg, Gojenbergsweg 112, 21029 Hamburg, Germany (svrielmann@hs.uni-hamburg.de)*

<sup>3</sup>*W&B Observatory, P.O. Drawer 1130, Cloudcroft, NM 88317, USA (offutt@apo.nmsu.edu)*

30 October 2018

## ABSTRACT

We present an Eclipse Mapping analysis of ten eclipses taken during decline from superoutburst of the dwarf nova V2051 Oph. On decline from superoutburst the disc cools down considerably from nearly 50,000 K in the intermediate disc ( $\sim 0.2R_{L1}$ ) near maximum to about 25,000 K at the end of our observing run, i.e. within 4 days. The average mass accretion rate through the disc drops in the same time from  $10^{18}$   $\text{gs}^{-1}$  to below  $10^{17}$   $\text{gs}^{-1}$ .

While in some maps the brightness temperature follows the steady state model, in others the temperature profile shows flattenings and/or indication of an inward travelling cooling front with a speed of approximately  $-0.12$   $\text{km s}^{-1}$ , possibly a reflected heating front with a speed of  $+1.8$   $\text{km s}^{-1}$  and a newly reflected cooling front with the same speed as the first one. Such scenario has been predicted (Menou et al. 2000) but not been observed before. Furthermore, we see a prograde precession of the enlarged disc with a precession period of about  $52.5^h$  in very good agreement with the independently determined superhump period observed by Kiyota & Kato (1998). At the same time, the uneclipsed component – presumably a disc wind – decreases significantly in strength during decline from superoutburst.

**Key words:** binaries: eclipsing – novae, cataclysmic variables – accretion, accretion discs – stars: V2051 Oph

## 1 INTRODUCTION

Cataclysmic variables (CVs) are close, interacting binaries in which a Roche-lobe filling main sequence star (the secondary) loses matter to its somewhat more massive white dwarf companion. In the absence of strong magnetic fields the angular momentum conservations leads to the formation of an accretion disc around the primary component through which the matter from the secondary is accreted onto the compact object. A detailed description of such systems is given in Warner (1995), an introduction in Hellier (2001).

If the mass transfer rate is below a certain limit, these discs undergo outbursts, during which the system brightens by a few magnitudes. The cause of such outbursts is the accumulation of material in the disc leading to a temperature increase and subsequently ionization of hydrogen. The changed opacity leads to a sudden further increase in temperature. The system is in outburst. However, with such a low mass accretion rate as is typical for a dwarf nova this state cannot be maintained. Subsequently, due to a decrease in surface density and temperature the hydrogen eventually

recombines and the disc returns to its pre-outburst, quiescent state. Osaki (1996) gives an overview on mechanisms and outburst types.

Certain CVs additionally show so-called superoutbursts. These outburst last longer than normal outbursts, but show a similar maximum brightness. Additionally, they are associated with so-called superhumps, short brightenings with a period slightly dissimilar to the orbital period. The superoutbursts are usually associated with the accretion disc’s apsidal precession (see e.g. Patterson et al. 2002).

The eclipsing cataclysmic variable V2051 Oph was discovered by Sanduleak (1972). Only few outbursts of the system have been reported (Warner & O’Donoghue 1987, Warner & Cropper 1983, Bateson 1980) with a maximal magnitude in B of about 13 in September 1980, possibly in April 1982 and in May 1984. It is possible that outbursts were missed due to the faintness of the system (Wenzel 1984). In May 1998 the first superoutburst was detected (Kiyota & Kato 1998).

We observed V2051 Oph during this superoutburst between maximum and near quiescence. This paper presents an analysis of these data using the Eclipse Mapping technique invented by Horne (1985).

\* Send offprint requests to: S. Vrielmann

Pass band response function for #21 Orange filter

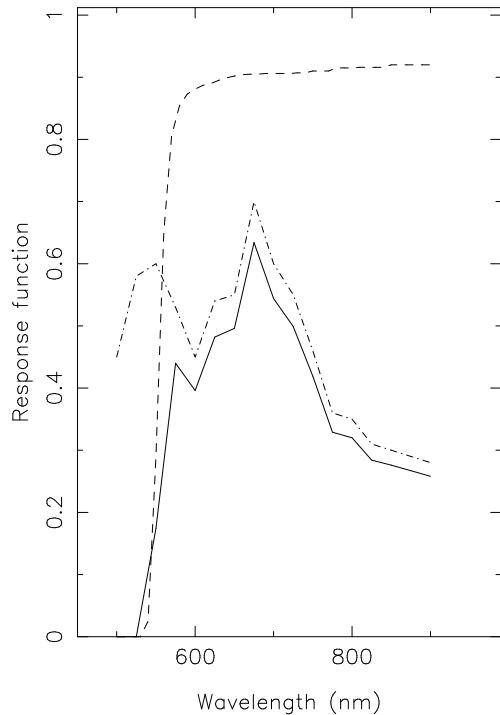


**Figure 1.** The pass band response functions for the #21 Orange filter (dashed line) and the TC-241 CCD chip (dashed-dotted line) as well as the product of both response functions (solid line).

**Table 1.** The superoutburst light curves of V2051 Oph.

local evening date	HJD(start)	Eclipse No.
23/5/98	2450957.24170	S01, S02, S03
25/5/98	2450959.24344	S33, S34
26/5/98	2450960.23838	S49, S50, S51
27/5/98	2450961.22460	S65, S66

## 2 THE DATA

Our observing set consists of 10 eclipses taken in four nights between 23 and 27 May 1998 (interrupted by a cloudy night) during the superoutburst first reported by R. Stubbings through VSNET. The data were gathered by W. Offutt with the 60cm Ritchey-Chretien telescope at the W&B observatory in New Mexico/USA using a #21 Orange filter which covers R band and the long wavelength region of the V band, see Fig. 1. For reasons described in Section 2.1 the eclipse light curves were not averaged or phase binned, but left at the original phase resolution of 10 to 15 sec (about 0.0023 in phase). A log of the superoutburst data is shown in Table 1.

According to VSNET observers the superoutburst started on May 17 when the system rose to a magnitude of 13.5. It reached the maximum on May 18 with a magnitude of 11.7 and ended after May 27. Since this system in quiescence is usually too faint for amateur astronomers it is not possible to pin down the exact length of the outburst or even get a complete superoutburst light curve.

Our series therefore started during decline of the superoutburst and ended when the system got too faint for the

telescope with the given filter. This means we did not cover the full decline, but only down to near the quiescent state.

For the phasing of the data we used the ephemeris of Echevarría & Alvarez (1993). Since the white dwarf is most certainly outshone by the accretion disc and due to the irregular eclipse profile (see following Section) we did not attempt to determine a new ephemeris from these superoutburst data.

### 2.1 The light curves

Fig. 2 shows the observed eclipse light curves. A preliminary analysis of the superoutburst data was shown in Vrielmann & Offutt 1999. But in that case we averaged the light curves of each night, losing information about the short term variation of the disc.

As can be seen in Fig. 2, the out-of-eclipse levels and the eclipse profile change dramatically throughout the four nights. The out-of-eclipse level drops from about 35 mJy down to 10 mJy and the eclipse minimum appears at positive or negative phases. The shifts in eclipse minimum indicate that the disc brightness distribution is asymmetric during superoutburst, with occasionally the leading or the following lobe of the disc being brighter.

The eclipse shape is sometimes symmetric (as in eclipses S01, S49, S50, S51 and S65) and in other cases very asymmetric with out-of-eclipse levels before eclipse being higher (S02,S03,S66) or lower (S33,S34). These general differences will appear in the reconstructions as distinctive features.

## 3 THE ANALYSIS

### 3.1 Eclipse Mapping

The eclipse mapping technique was invented by Horne (1985) as a tomographic tool to reconstruct the intensity distribution in the accretion disc by fitting the eclipse profile. Thus, intensity maps of the accretion disc are derived using a maximum entropy algorithm (MEM, Skilling & Bryan 1984). The MEM algorithm serves to avoid the ambiguities of reconstructing a two dimensional map from a one-dimensional data set (the light curve) and introduces a certain degree of symmetry in the map<sup>†</sup>. Otherwise, a minimum of assumptions about the system are made as to minimally influence the results by premonitions.

The only assumptions are that the geometry of the system is known (e.g. the secondary star fills its Roche-lobe, the accretion disc is flat or of pre-determined 3-dimensional shape) and that the accretion disc is not changing during the course of the eclipse as any short term variation will lead to smeared out features in the reconstructions. While the first assumption is generally relatively well fulfilled, the latter assumption is usually not, since accretion discs show short-term fluctuations in brightness called flickering. In order to minimize this effect, usually a number of eclipse light curves are averaged.

<sup>†</sup> For the current mapping we used a solid arc smearing with smearing parameters  $0.1R_{L1}$  in radius and  $20^\circ$  in azimuth at the disc edge.

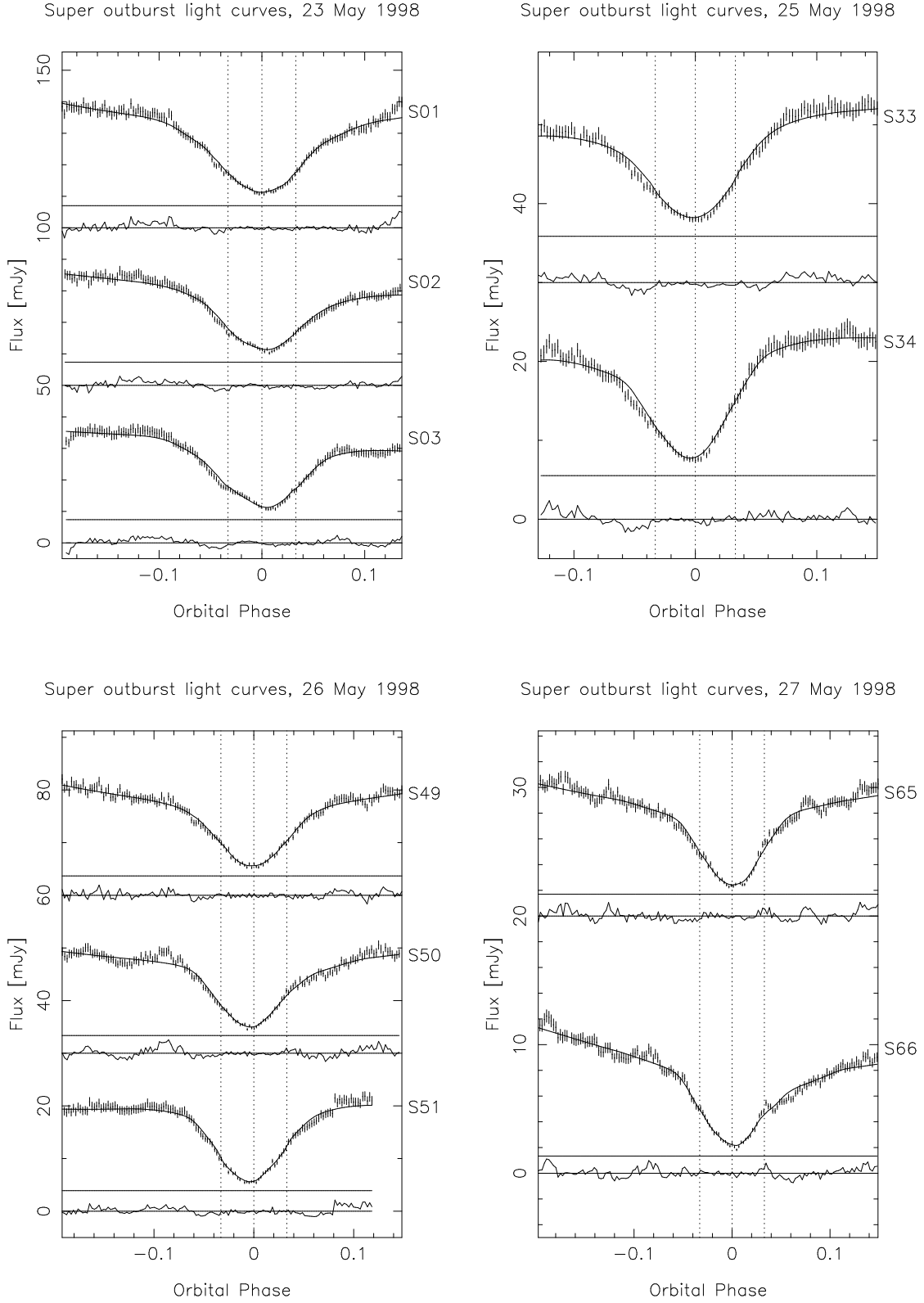


**Figure 2.** The 10 superoutburst light curves together with the PPEM fits. The eclipse light curve number is given on the right of each panel. Light curves are offset by 50mJy, 30mJy, 30mJy and 20mJy, respectively, for the four different nights with horizontal lines giving the zero-level for each light curve. The residuals for each light curve cross the zero-level lines. Additional horizontal solid lines indicate the reconstructed flux of the uneclipsed component (see also Fig 6 and Table 2). Dashed vertical lines indicate phase 0 and the ingress and egress phases of the white dwarf at -0.033 and 0.033 for comparison.

In the present case we did not average the eclipse light curves, because we were interested in possible changes in the disc between eclipses, e.g. due to a precession of the disc. The precession may cause a change of the orientation of the elliptical disc between two consecutive eclipses. Therefore, we do not want to lose this information by averaging over the eclipse light curves of a specific night. This means, on the other hand, that we have to be careful not to over-interpret structures in the light curve which are due to flickering.

### 3.2 The system parameters

The inclination angle  $i = 83.3^\circ$ , the mass ratio  $q = 0.19$ , the white dwarf mass  $M_{wd} = 0.78M_\odot$  and radius  $R_{wd} = 0.0244R_\odot$  as well as the scale parameter  $R_{L1}/R_\odot = 0.42$  were taken from Baptista et al. (1998). For the distance we used the Physical Parameter Eclipse Mapping estimate by Vrielmann, Stiening & Offutt (2002) of 146 pc.

### 3.3 The disc geometry

In a first attempt to reconstruct the outburst disc we used a geometrically infinitesimally thin disc in the orbital plane. However, the disc appeared to be bright in the back part (disc region opposite the secondary star) – showing a so-called back-to-front asymmetry –, indicating that the disc has a certain, non-negligible thickness. This can also be seen in Z Cha during outburst (Robinson, Wood & Wade 1999). Therefore, for the study of the outburst disc we use a 3-dimensional disc geometry.

We constructed a circular disc geometry with a fixed opening angle. At the edge we allowed emission to be reconstructed on a vertical ribbon around the disc. This geometrical model introduces two new parameters, the opening angle and the disc radius (or disc size). However, it turned out that the exact value of the opening angle did not influence the results dramatically. Similar results were found by Robinson et al. (1995) and Robinson (1999, private communication).

Since we used an inclination angle of  $i = 83.3^\circ$ , we arbitrarily chose a half opening angle of  $\alpha = 6.7^\circ$  (which allows us to see just about all parts of the disc and the white dwarf) and a somewhat smaller angle of  $\alpha = 4^\circ$ . A comparison of the reconstructions showed that in almost all cases the entropy corresponding to the maps with the larger angle is somewhat larger than the entropies for the thinner disc. In the remaining cases (eclipses S01, S34, S51) the entropies of the reconstructions of both angles were almost identical. Therefore we chose the larger angle of  $\alpha = 6.7^\circ$ .

Using a fixed opening angle means introducing an edge of the disc in the form of a ribbon around the disc perimeter with 126 pixels onto which intensity could be reconstructed as well as onto the circular disc surface. This ribbon is set vertical to the orbital plane around the disc at the disc edge  $R_e$ , therefore we can identify the ribbon pixel uniquely by their azimuthal angle. We see at most half of this ribbon, which half depending on the orbital phase. During eclipse, a further part of this ribbon is occulted by the secondary. A similarly flared disc geometry was used by Bobinger et al. (1997).

Since the 3:1 resonance radius in V2051 Oph's accretion disc lies at  $R_{3:1} = 0.68R_{L1}$ , the superoutburst disc is

expected to be larger than this. On the other hand, the Roche-lobe of the primary confines the disc to within about  $R_R = 0.8R_{L1}$ . We chose a disc edge at  $R_e = 0.7R_{L1}$ .

If the radius  $R_e$  is chosen too small we should see this as enhanced emission from the outer regions of the disc; if it is too large, the reconstructions simply should not show much intensity in the outer regions of the disc. Therefore, since the range between  $R_{3:1}$  and  $R_R$  is small, the exact choice will not influence our results dramatically. However, because of the MEM algorithm used in Eclipse Mapping, the reconstructed brightness distribution in the disc – especially close to the disc edges – is severely smeared out (see also Appendix A) and will not be affected by a small difference in true to assumed radius.

The introduction of a ribbon allowed us to use the light curves as they were, without levelling the out-of-eclipse light curves. A flat disc geometry cannot cope with different out-of-eclipse levels, but in the flared disc approach intensity can be reconstructed onto the ribbon. For example an orbital hump can be reconstructed on the leading side of the ribbon, very well visible before eclipse and more or less invisible after. However, in the present case we are dealing with superoutburst data. We can therefore not distinguish between an orbital hump and a superhump – especially since our observations only cover the immediate eclipses. Nevertheless, we did not attempt to level out the out-of-eclipse light curves.

The use of a circular disc geometry seems to contradict the expectation for a precession of the disc with an elongated, elliptical disc shape. However, in order to avoid any assumption about the direction of the semi major axis in the disc, we use a circular disc geometry. In the case that the disc is truly elongated, we will face similar scenarios as described above for a too small or too large  $R_e$ , this time only applying to parts of the disc, i.e. we would either see a lack of emission or enhancement close to the edge of two regions  $180^\circ$  apart from each other.

To identify the location of structures in the disc we use the radius and azimuth. Azimuth  $0^\circ$  indicates the direction from the white dwarf to the secondary, negative azimuths correspond to the following lune, positive angles to the leading lune of the accretion disc (the side where the accretion stream hits the disc).

### 3.4 The maps

The Eclipse Mapping fits to the light curves (Fig. 2) are good, we reached a  $\chi^2$  of 1 for all light curves except for light curves S50, S65 and S66 where we aimed only at a  $\chi^2$  of 1.5 instead of 1. Aiming at a lower  $\chi^2$  would have led to artificial structures and noise in the maps.

Since the outburst disc is usually optically thick, the reconstructed brightness distribution can directly be translated into a map of the brightness temperature and treated as good approximations of the true disc temperatures.

The disc reconstructions are displayed in Fig. 3. The inner disc appears to be very hot on the first night, with temperatures up to 100 000 K in the disc centre and around 50 000 K in the intermediate disc ( $\sim 0.2R_{L1}$ ). The temperature drops in the following nights to values around 30 000 K on May 25 and 26 and 20 000 K in the last night within a radius of about  $0.2R_{L1}$ . These values are compatible with

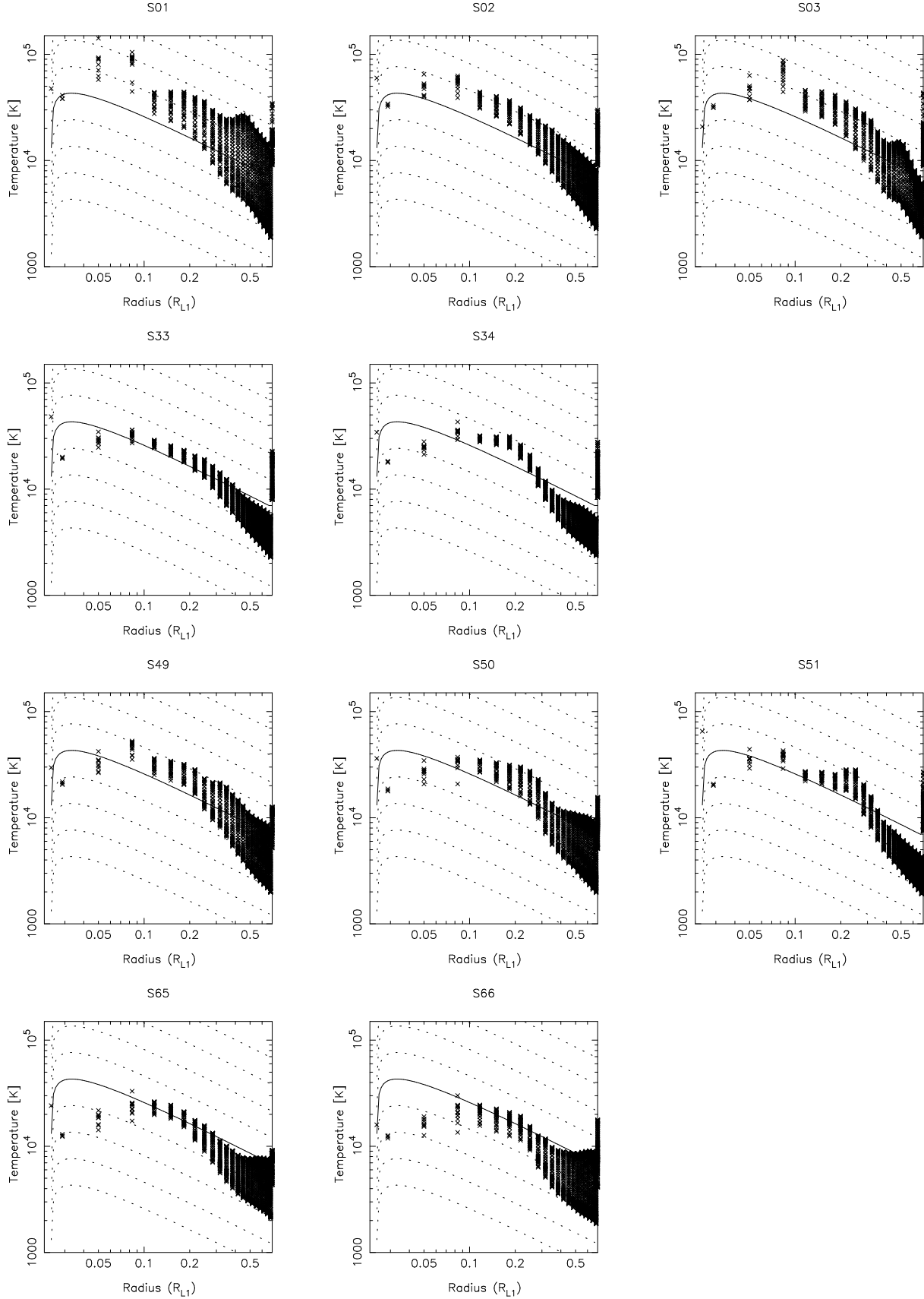


**Figure 3.** The brightness temperatures of the four superoutburst nights in the thick disc approximation. The number of the corresponding eclipse light curve is given above each panel. (The eclipses corresponding to the maps in the each column are separated by multiples of almost exactly  $24^h$ .) The panels show radial brightness temperatures in the disc and the ribbon (at radius  $0.7R_{L1}$ ). Underlying dashed lines are theoretical steady state distributions for mass accretion  $\log \dot{M} = 13$  to  $21$ , the one for  $\dot{M} = 10^{17} \text{gs}^{-1}$  is drawn solid for comparison of the four plots. Temperatures of about 5000 K or below correspond to regions with no significant emission. The scale is the same in all plots.

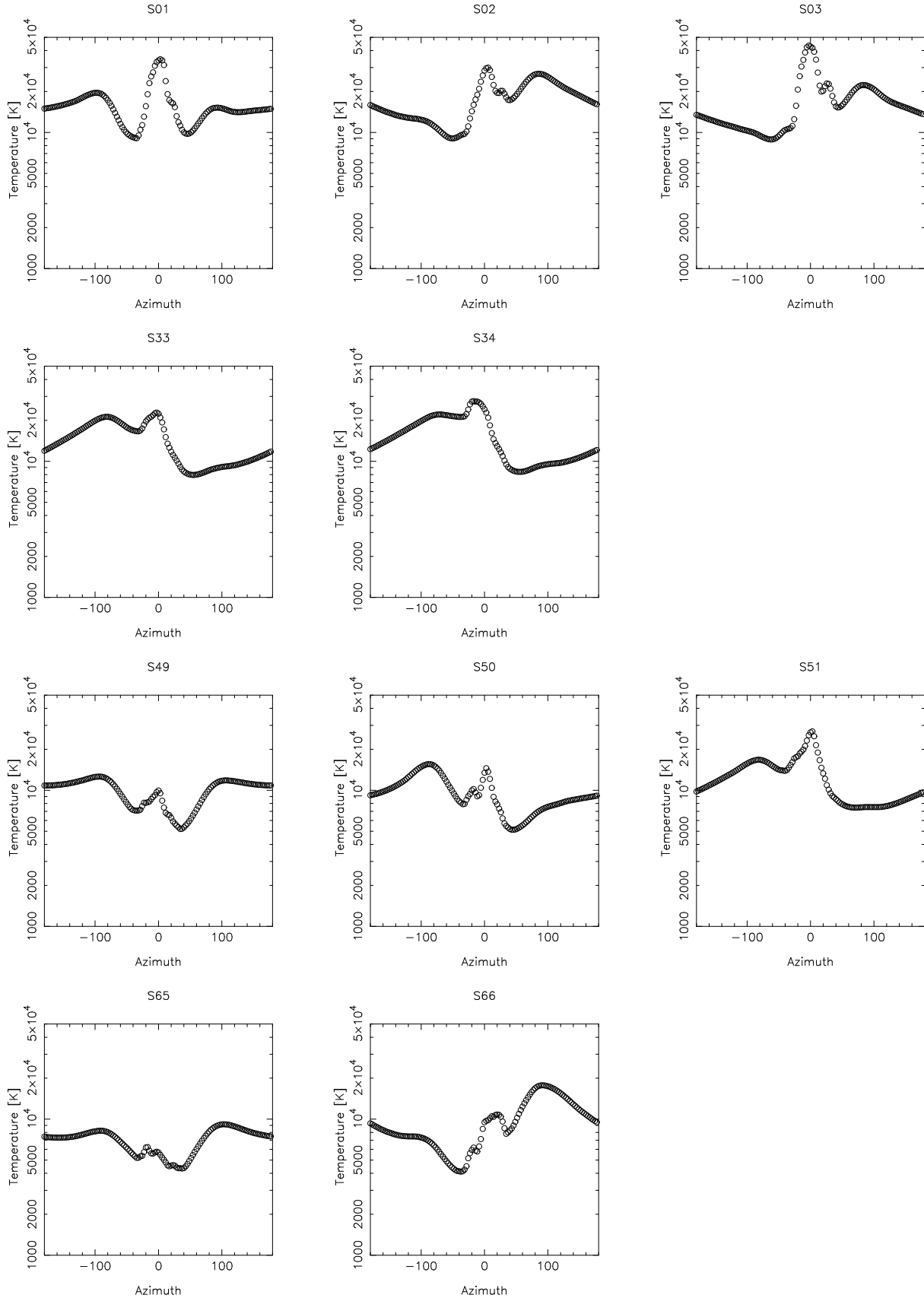


**Figure 4.** The brightness temperatures on the ribbon during the four superoutburst nights. The number of the corresponding eclipse light curve is given above each panel. The azimuth  $0^\circ$  corresponds to the point closest to the secondary,  $\pm 180^\circ$  to the point farthest away from the secondary. While a small scale variation may be an artefact, one can distinguish a component with an apparent movement from the leading side (positive angles) to the trailing side (negative angles) of the disc during the first three nights. Temperatures of about 5000 K or below correspond to regions with no significant emission. The scale is the same in all plots.

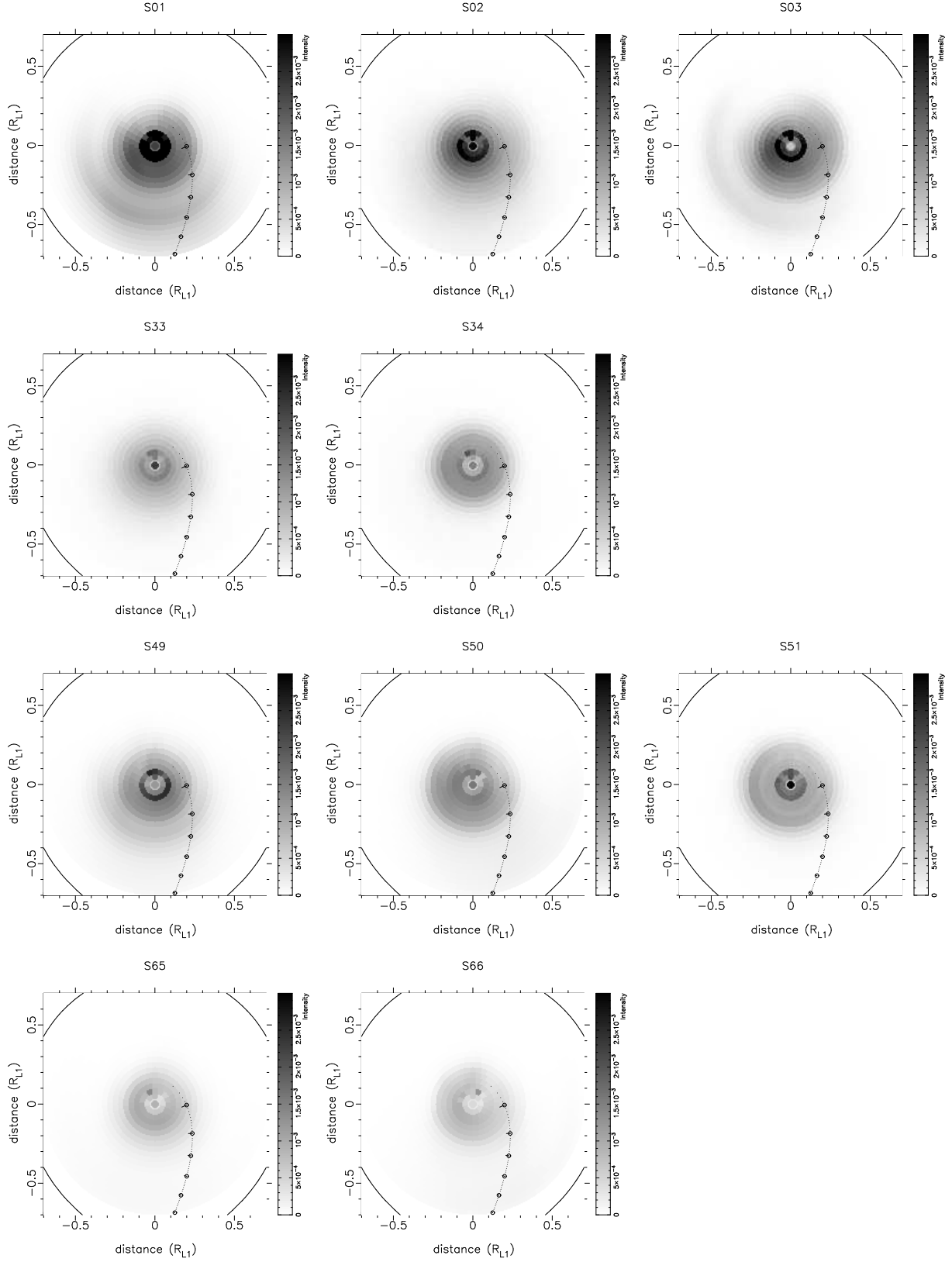


**Figure 5.** The reconstructed intensity distributions for the superoutburst disc as grey-scale plots. The number of the corresponding eclipse light curve is given above each panel. Parts of the Roche-lobe are plotted as a solid line and ballistic streams for a mass ratio  $q = 0.19$  as dotted lines with the secondary positioned below the plot, outside the plotted region. (The intensity in the ribbon is not plotted, since it would not give more information than Fig. 4.) The scale is the same in all plots for comparison. It is set to an “overexposure” in the maps of May 23rd to enhance the outer regions of the disc of the first night and to allow the discs of the last night to be visible. (The maximum of the intensity scale is lower than the maximum in the intensity values of the maps in the first night.)

theoretical considerations (Smak 2000, Menou, Hameury & Stehle 1999).

In the intermediate disc the temperature either follows a steady state distribution (e.g. S02, S33, S49, S66) or is flat (S34, S51) or inbetween. The mass accretion rate in the former cases is about  $10^{18} \text{ gs}^{-1}$  in S02,  $3 \times 10^{17} \text{ gs}^{-1}$  in S33,  $5 \times 10^{17} \text{ gs}^{-1}$  in S49 and  $10^{17} \text{ gs}^{-1}$  in S66. The last value is about a magnitude above the quiescence value of  $10^{16} \text{ gs}^{-1}$  (Vrielmann et al. 2002).

Fig. 4 shows the temperature distribution along the ribbon. A comparison with Fig. 3 shows that the reconstructed temperature in this ribbon is significantly higher than in the disc edge and in some cases comparable to the temperature at a radius of about  $0.2R_{L1}$ . As such feature does not appear in the test cases, it is unlikely to be a systematic effect caused by the method. It is possible that this indicates that the opening angle of the disc is chosen too small, thus concentrating the emission on a too small surface at the disc edge. Furthermore, this would mean that parts of the disc surface are eclipsed by the high disc edge. As the jump is strongest in those eclipses which show the strongest asymmetry (i.e. S02, S03, S33, S34, with the exception of S51) this might indicate an uneven height of the disc edge and a variability of the flaring angle during the course of the decline.

While for each night the distribution is similar, large differences appear for different nights, reflecting a slow but significant change of the disc. In Section 4.2 we describe what we can learn from these plots.

The grey-scale plots in Fig. 5 give some indication of the emissivity and possibly shape of the disc. However, since the MEM algorithm introduces a certain amount of radial and azimuthal smearing (and therefore a certain amount of symmetry) and due to a fixed circular geometry we will not necessarily be able to directly reconstruct an elliptical disc. A comparison to the test case in Appendix A, however, shows that in all maps we can see an asymmetry possibly indicating an elliptical – definitely non-circular – intensity distribution. The fact that in the maps the “front” instead of the “back” part is bright might indicate that the opening angle we chose is too large, however, the bright region is not always symmetric around azimuth  $0^\circ$ .

An interesting feature is the arc like structure in S01 and S03 and possibly S49 (merged with the central part of the disc). Similar structures have been observed in IP Peg during decline from outburst (Vrielmann 1997).

### 3.5 The uneclipsed component

Table 2 and Fig. 6 give the reconstructed uneclipsed component in the #21 Orange filter for the observed outburst nights. The scatter of the uneclipsed flux values in each night is an indication for the error of these values of roughly half a mJy. The flux level drops dramatically during the four nights. Since the filters R and #21 Orange are similar, one can compare this flux with the uneclipsed quiescent flux in the R band of 0.66 mJy (see Vrielmann et al. 2002). This indicates that even in the fourth night the uneclipsed light was not yet at its quiescent level.

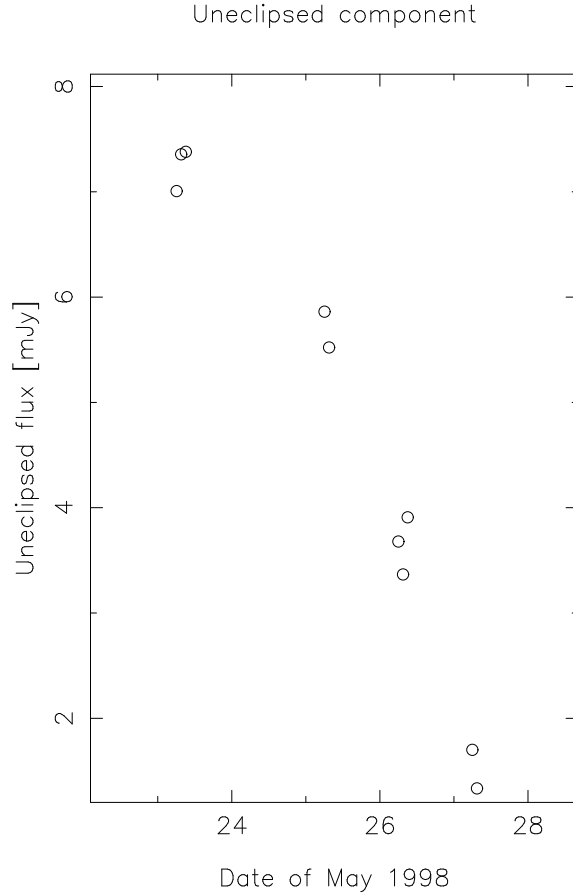


**Figure 6.** The uneclipsed component during the four superoutburst nights (cf. Table 2).

**Table 2.** The reconstructed flux for the uneclipsed component in the #21 Orange filter for the four superoutburst nights.

Eclipse no.	Night (Date of May)	Time of mid-eclipse (in fractions of HJDs)	Flux (mJy)
S01	23	.2538	7.01
S02		.3162	7.36
S03		.3787	7.38
S33	25	.2515	5.86
S34		.3139	5.52
S49	26	.2503	3.68
S50		.3128	3.37
S51		.3752	3.91
S65	27	.2492	1.70
S66		.3116	1.33

## 4 DISCUSSION

### 4.1 The disc evolution during superoutburst

Assuming that in superoutburst the disc emits as an optically thick source, we derive brightness temperatures from observations in an orange filter (part of V and up to I). The reconstructed maps show that the disc cools down considerably during the four nights.

Only in the intermediate eclipses (i.e. S34, S49, S50, S51, S66) do we see indications for a cooling front as

expected by theoretical calculations (e.g. Cannizzo 1993). Measuring the location of the cooling front in S34 and S49 we derive a speed of  $-0.12 \text{ km s}^{-1}$ , measuring the speed of the cooling front between S51 and S66 we also derive a speed of about  $-0.12 \text{ km s}^{-1}$ , whereas these two cooling fronts are not identical.

These speeds are comparable to the value Menou et al. (1999) found with numerical simulations and who predict a fraction of a  $\text{km s}^{-1}$ . Furthermore, it is comparable with the speeds derived with Eclipse Mapping of  $-0.43$  to  $-0.06 \text{ km s}^{-1}$  for EX Dra (decreasing during outburst, Baptista & Catalàn 2001), of  $-0.8 \text{ km s}^{-1}$  for IP Peg (Bobinger et al. 1997) and  $-0.7$  to  $-0.14 \text{ km s}^{-1}$  for OY Car in superoutburst (Bruch, Beele & Baptista 1996).

Now, why do we see two distinctly different cooling fronts? The explanation can be found in numerical calculations by e.g. Menou et al. (2000) who find that an inward moving cooling front can reflect an outward moving heating front which again reflects into an inward moving cooling front. If we assume this scenario we derive a speed of  $+1.8 \text{ km s}^{-1}$  for the reflected heating front. A speed of a few  $\text{km s}^{-1}$  is typical for heating fronts (Menou et al. 1999). Furthermore, the reflection of the heating front occurs at a disc radius  $R_{front}$  of about  $4 \times 10^9 \text{ cm}$ , compatible with Menou et al.'s (2000) finding that they occur at  $R_{front} \lesssim 10^{10} \text{ cm}$  in their simulations.

If such multiple reflections of cooling and heating fronts do occur in V2051 Oph, we should observe re-flares as predicted by numerical simulations (Menou et al. 2000). Unfortunately, the coverage of this object by amateur astronomers (VSNET, AAVSO) during the so far observed superoutbursts is too sparse to confirm or reject the appearance of re-flares. Detailed observations during the next super outburst are highly desirable.

## 4.2 The disc precession

During superoutburst, we see a partially strong, variable peak in the intensity distribution on the edge of the disc. It is probably caused by an elliptical, precessing disc: Whenever one of the vertices of the semimajor axis of the disc is close to the secondary, the disc will experience tidal forces leading to precession and local heating of the disc. The disc will react on the temperature increase by flaring up near the secondary. So, the location of the peak gives a rough estimate for the phase of the apsidal precession. In Appendix A we show that the location of a bright area (not to be confused with the bright spot) on the disc edge can be relatively well determined.

Looking at the distribution of light along the rim of the disc, we identify three structures present in most reconstructions: (a) a central peak close to azimuth  $0^\circ$  (facing the secondary); (b) a secondary peak in the profile of the central peak; and (c) a broad underlying brightness distribution with a maximum at  $90^\circ$  and/or  $-90^\circ$ . The latter peaks at the same side of the disc as the secondary peak is located. Similar features appear in the test (Appendix A).

The central peak is also present in the test cases and therefore most likely an artefact, although it could also be associated with the bright spot where the ballistic stream hits the accretion disc. Such a spot was not considered in the test case. The location of the bright spot is only marginally

influenced by a apsidal motion of an elliptical, precessing disc. As apparent from the tests, the large scale variation on the disc rim is most likely an artefact.

If we measure the position of the second peak, we find a  $10^\circ$  prograde shift per eclipse or a  $10\text{-}20^\circ$  backwards shift per day. If this can be considered an indication for the apsidal motion of the disc, we arrive at a value for the precession period  $P_{prec}$  of  $51^h$  to  $54^h$ , slightly larger than two days (therefore the apparent backward shift during consecutive nights). This would mean the disc is slightly larger than the 3:1 resonance radius  $R_{3:1}$  of  $0.68R_{L1}$  and the superhump period ( $P_{sh} = P_{prec}P_{orb}/(P_{prec}-P_{orb})$ , Warner 1995) should be 2.5 min or 3% larger than the orbital period  $P_{orb} = 1.4982$  hours, i.e.  $P_{sh}(\text{predicted}) = 1.5422^h \pm 0.0013^h$ . This is in very good agreement with the superhump period of  $0.06423^d = 1.54152^h$  independently determined by Kiyota & Kato (1998) during the same super outburst.

This value for the precession period is very typical for SU UMa type dwarf novae, e.g. DV UMa ( $67^h$ , Patterson et al. 2000), HT Cas ( $52^h$ ), Z Cha ( $51^h$ ), OY Car ( $65^h$ ), IR Gem ( $47^h$ ), AQ Eri ( $52^h$ ) to name but a few or even the nova V1974 Cyg with  $44^h$  (Retter, Leibowitz & Ofek 1997). Numerical calculations of super outbursts of dwarf novae with a similar mass ratio as V2051 Oph give on average a slightly larger ratio of  $P_{sh}/P_{orb}$  of about 1.06 (Murray 1998) compared to our 1.03.

## 4.3 The mass accretion rate

The mass accretion rate  $\dot{M}$  in superoutburst appears very high, around  $10^{18} \text{ gs}^{-1}$  in our first night and varying throughout the disc. This is about two magnitudes larger than in quiescence (about  $10^{16} \text{ gs}^{-1}$ , Vrielmann et al. 2002). Towards the end of our observing run (somewhat before the end of the outburst) the disc cools down and shows a mass accretion rate of about  $10^{17} \text{ gs}^{-1}$ , still a magnitude higher than the quiescent level.

Only occasionally the disc appears to follow the steady state models and then only in intermediate disc regions between  $0.1R_{L1}$  and  $0.2R_{L1}$ . At other times the distribution is rather flat. During the last eclipse, when the disc is near the quiescent level, indication for a bright spot can be seen at the expected location where the accretion stream hits the disc.

Since the disc undergoes dramatic changes during the course of an outburst with cooling fronts travelling through the material, we would not expect it to settle down completely into a steady state. However, the fact that parts of the disc do seem to appear in steady state suggests that the time scale for returning into the steady state is relatively short, of the order of a day or less.

According to Tylenda's (1981) calculations, the mass accretion rate in superoutburst is too high and the disc is too small (outer radius at  $2.3 \cdot 10^{10} \text{ cm}$ ) to show optically thin areas – the disc should be everywhere optically thick. This agrees very well with our assumption to consider the brightness temperatures as good approximations of the gas temperatures.

#### 4.4 The disc wind

The Eclipse Mapping shows that the uneclipsed component is decreasing in strength on decline from outburst, but never disappearing completely, as the analysis of the quiescence data show (Vrielmann et al. 2002). A similar variability has been found for EX Dra by Baptista & Catalán (1999) where the out-of-eclipse flux in R dropped during decline from outburst and practically disappeared at minimum light. At that time EX Dra's disc is reduced to the immediate vicinity of the white dwarf. Baptista & Catalán suggest this variable part of the uneclipsed component is due to a disc wind and a chromosphere ejected by the inner part of the disc. The variation in these components is presumably due to a variable mass accretion rate.

Our geometrical model of the superoutburst disc is very simple; the disc may in fact be thicker, tilted, warped or only flare close to the secondary. The latter geometrical model would introduce too many free parameters (extent and location of flared part) which we cannot determine from our data. However, the uneclipsed component is a flux independent of orbital phase and therefore unlikely to originate in the (eclipsed parts of the) disc itself, but rather in a region above the disc. The easiest explanation is the same as for EX Dra: a variable disc wind triggered by the outburst.

#### ACKNOWLEDGMENTS

We thank all amateur astronomers who are dedicating much of their spare time to continuously monitor dwarf novae in order to detect outbursts. SV is funded by the South African Claude Harris Leon Foundation through a postdoctoral fellowship.

#### REFERENCES

- Baptista, R., Catalán, M.S. 1999, In: "Cataclysmic Variables: a 60th Birthday Symposium in Honour of Brian Warner", Warner Symposium Proceedings, Oxford, April 12-17 1999, ed. P. Charles, A. King, D. O'Donoghue, New Astronomy Reviews, Elsevier Science, p. P1 (also at astro-ph/9905096)
- Baptista, R., Catalán, M.S. 2001, MNRAS, 324, 599
- Baptista, R., Catalán, M.S., Horne, K., Zilli, D. 1998, MNRAS, 300, 233
- Baptista, R., Steiner, J.E., Cieslinski, D. 1994, ApJ, 433, 332
- Bateson, F.M. (ed.) 1980, Var. Star. Circs. R. astr. Soc. N. Zealand
- Bobinger A., Horne K., Mantel K.-H., Wolf S. 1997, A&A 327, 1023
- Bruch, A., Beele, D., Baptista, R. 1996, A&A, 306, 151
- Cannizzo, J.K. 1993, in Accretion Discs in compact systems, ed. J.C. Wheeler, Advanced Series in Astrophysics and Cosmology, Vol. 9, World Scientific, London
- Echevarría, J., Alvarez, M. 1993, A&A, 275, 187
- Hellier, C. 2001, "Cataclysmic variable stars – How and why they vary", Springer-Praxis Books in Astronomy and Space Sciences
- Horne K., 1985, MNRAS 213, 129
- Kiyota, S., Kato, T. 1998, IBVS, No. 4644
- Menou, K., Hameury, J.-M., Stehle, R. 1999, MNRAS, 305, 79
- Menou, K., Hameury, J.-M., Lasota, J.-P., Narayan, R. 2000, MNRAS, 314, 498
- Murray, J.R. 1998, MNRAS, 297, 323
- Osaki, Y. 1996, PASP, 108, 390
- Patterson J. et al. 2000, PASP, 112, 1584
- Patterson J. et al. 2002, PASP, 114, 721
- Retter, A., Leibowitz, E.M., Ofek, E.O. 1997, MNRAS, 286, 745
- Robinson, E.L., Wood, J.H., Wade, R.A. 1999, ApJ, 514, 952
- Robinson, E.L., Wood, J.H., Bless, R.C., Clemens, J.C., Dolan, J.F., Elliot, J.L., Nelson, M.J., Percival, J.W., Taylor, M.J., van Citters, G.W., Zhang, E. 1995, ApJ 443, 295
- Sanduleak, N. 1972, IBVS, No. 663
- Skilling J., Bryan R.K., 1984, MNRAS 211, 111
- Smak, J. 2000, Acta Astr., 50, 399
- Tylenda, R. 1981, Acta Astron., 31, 127
- Vrielmann, S. 1997, Ph.D. thesis, University of Göttingen
- Vrielmann, S., Offutt, W. 1999, in "Cataclysmic Variables: a 60th Birthday Symposium in Honour of Brian Warner", Oxford, April 12-17 1999, ed. P. Charles, A. King, D. O'Donoghue, New Astronomy Reviews, Elsevier Science, p. 39
- Vrielmann, S., Stiening, R., Offutt, W. 2002, MNRAS, 334, 608
- Warner, B. 1995, "Cataclysmic variable stars", Cambridge Astrophysics Series, Cambridge University Press
- Warner, B., Cropper, M. 1983, MNRAS, 203, 909
- Warner, B., O'Donoghue, D. 1987, MNRAS, 224, 733 (WO)
- Wenzel, W. 1984, IBVS, 2481, 1

#### APPENDIX A: TEST FOR RECONSTRUCTING ELLIPTICAL DISCS

In order to test how well an elliptical accretion disc can be reconstructed, we performed a test in which we constructed an artificial elliptical disc with an azimuthal angle of the semimajor axis of  $-20^\circ$  and a bright area at the vertex of the semimajor axis closest to the secondary (see Fig. A1 (*left*)). This bright area is a simple simulation of the flaring of the disc near the secondary. The geometry of the disc surface is the same as that described in Section 3.3.

For this artificial disc we calculated the light curve (see Fig. A2) that is to be fitted with the Eclipse Mapping algorithm. Artificial noise with a signal-to-noise level of 100 has been added to the light curve. This so constructed light curve shows a clear asymmetry with different slopes for the ingress and egress, different out-of-eclipse levels before and after eclipse as well as a minimum at a phase  $\neq 0$ . These features are also apparent in the superoutburst light curves of V2051 Oph (Fig.2).

The application of the Eclipse Mapping algorithm to these light curves lead to the reconstructed maps in Fig. A1 (*right*). On the surface of the disc only the "back" part of the disc (around an azimuth of  $160^\circ$ ) shows some brightening, the front part (around  $-20^\circ$ ) seems to be unchanged. This is probably due to a foreshortening of the front part of the disc because of the relatively large opening angle. In any case, the poor reconstruction of the elliptical shape in this test case means that we cannot expect to see an elliptical shape of the disc emission in Eclipse maps of observed light curves.

However, on the edge of the disc (the "ribbon") a brightening can be seen – even if much fainter than in the original map. In Fig. A3 we have plotted the light distribution along the disc edge for reconstructions using eight different orientation angles between  $0^\circ$  and  $35^\circ$ . For larger angles the flaring will be negligible.

Fig. A3 shows that in the reconstructions there is a large scale brightness variation, often a peak near azimuth

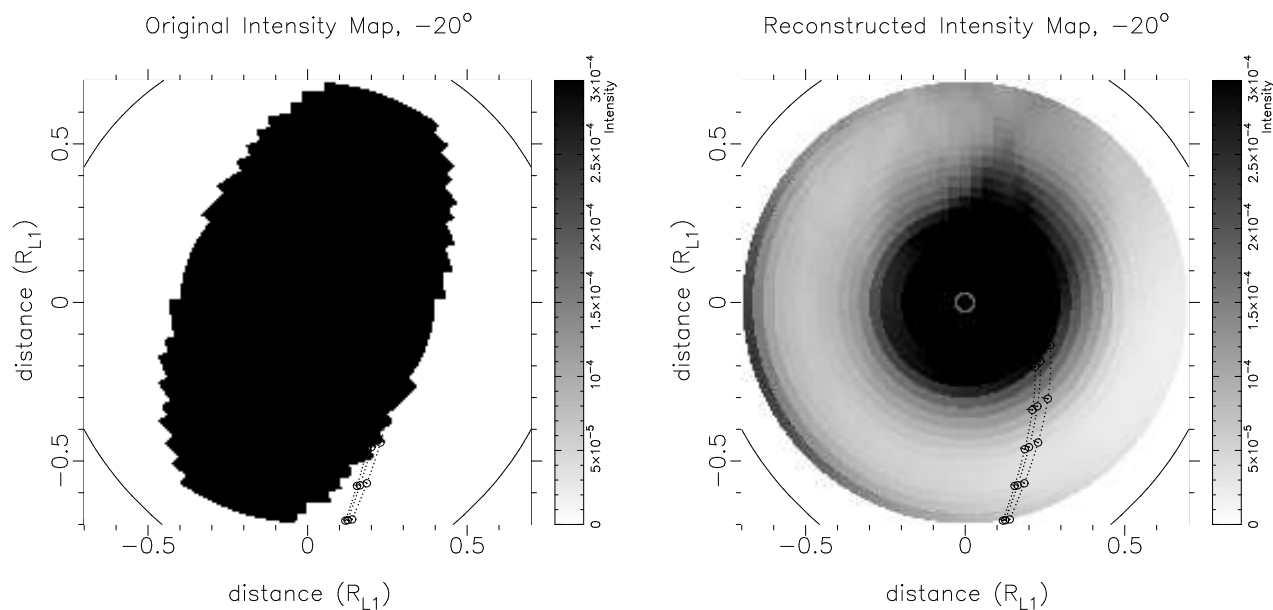


**Figure A1.** The original (*left*) and reconstructed (*right*) maps for the test case in which the accretion disc shows an elliptical intensity distribution on a circular disc geometry and has an orientation angle of  $-20^\circ$  in azimuth. The plots show the intensity map on the surface of the accretion disc. The solid line marks the Roche-lobe with the secondary being at the bottom, outside the plotted area; the dotted line indicates the theoretical mass accretion stream paths.

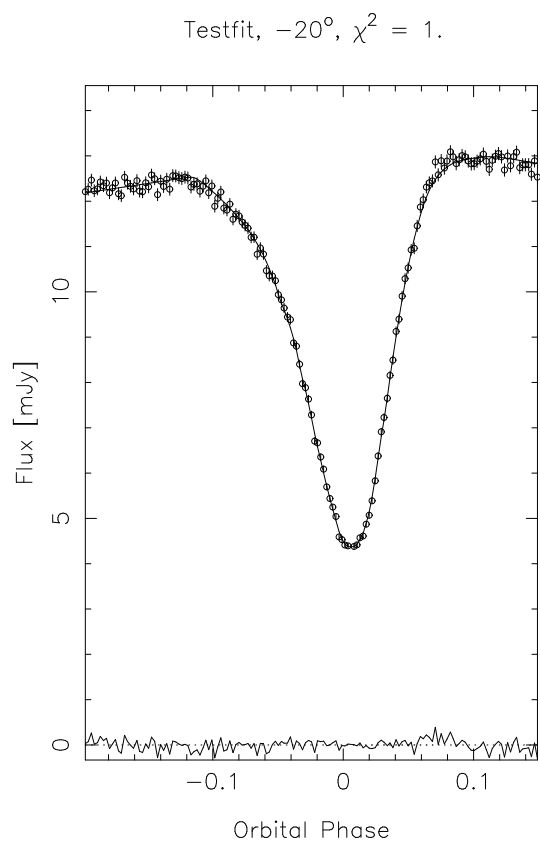


**Figure A2.** The light curve constructed from the artificial disc with the Eclipse Mapping fit (solid line through the data points) and the residuals (solid line around zero Flux level).

$0^\circ$  and for disc orientation angles  $> 10^\circ$  a peak that coincides well with the original position of the bright area on the disc edge. Although the reconstructed brightness distribution for a disc orientation angle of  $0^\circ$  is not similar to the original one, it is at least symmetric around azimuth  $0^\circ$ . For a disc orientation angle of  $5^\circ$  the reconstruction near azimuth  $0^\circ$  is rather noisy and should be recognizable in real data as a disc with an orientation angle close to  $0^\circ$ .

This test shows that a peak in the brightness distribution along the disc edge can be determined with a positional accuracy of  $5^\circ$ .

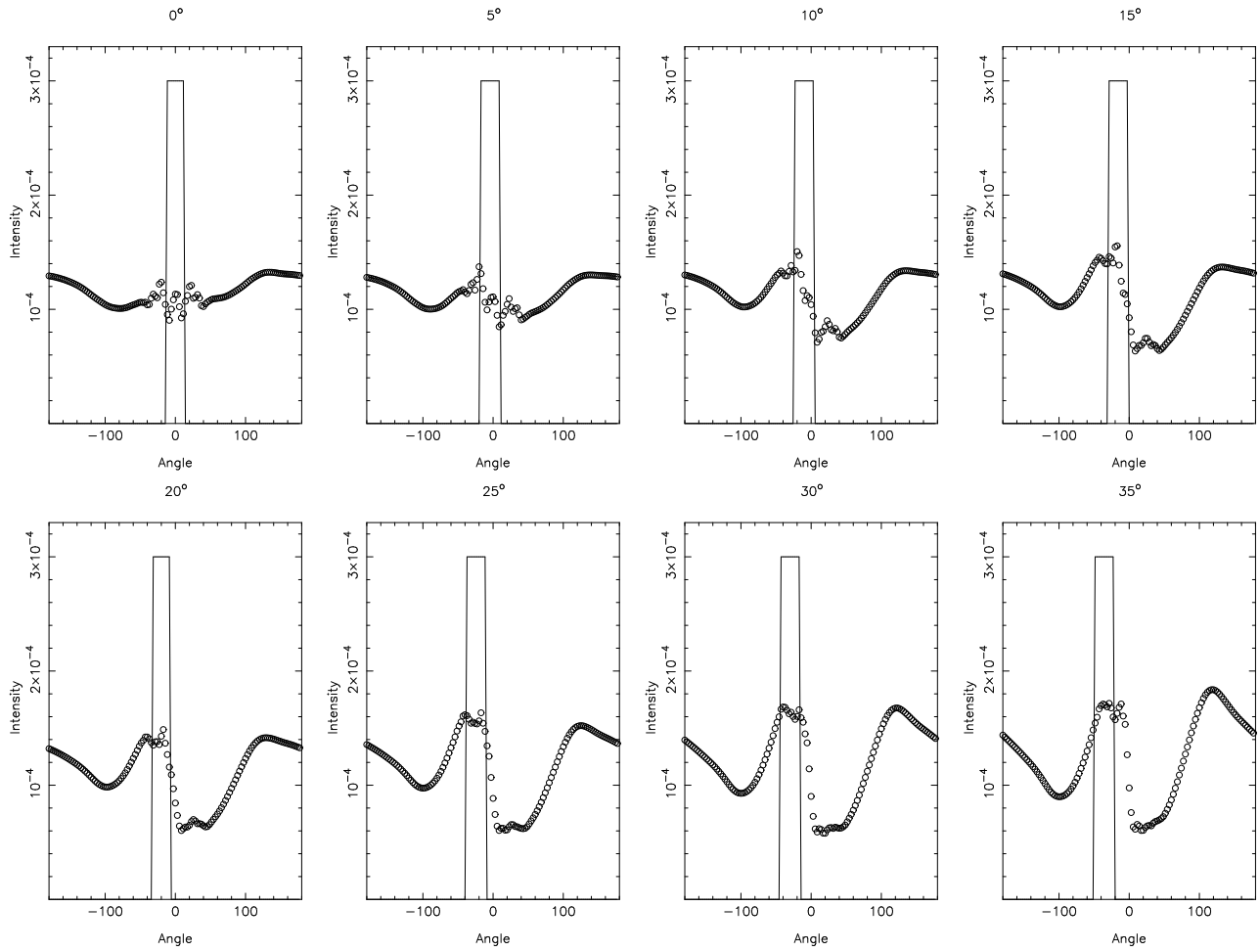


**Figure A3.** The reconstructed intensity distribution along the disc ribbon for 8 different accretion disc orientations (across and down) from  $0^\circ$  to  $35^\circ$  in  $5^\circ$  steps as indicated above each plot. The solid line indicates the position of the bright area on the disc edge and the circles the reconstructed brightness distribution.